PHYSICAL REVIEW B VOLUME 15, NUMBER 1 1 JANUARY 1977

Raman-scattering study of stress-induced ferroelectricity in $KTaO_3$

Hiromoto Uwe and Tunetaro Sakudo
Electrotechnical Laboratory, Tanashi, Tokyo, Japan
(Received 23 August 1976)

The stress-induced ferroelectricity in $KTaO_3$ is investigated by means of Raman scattering at 2 K. In the (010)-stress-induced ferroelectric phase, the transverse soft A_1, B_1, and B_2 modes have been observed as a first-order Raman scattering and are found to increase their frequencies with the stress in accordance with the Lyddane-Sachs-Teller relation. The A_1 Raman line is found to broaden as the stress approaches the transition stress. From the stress dependence of the soft-mode frequencies, the transition stress is estimated as 5.25 kbar in agreement with a previous dielectric observation. Values of the nonlinear dielectric susceptibilities are obtained from a comparison of a phenomenological theory to the experimental results. Furthermore, the effective charge of the soft mode is evaluated and the value is compared with previous data. From the first- and second-order Raman spectra up to 1200 cm^{-1}, zone-center phonons and pairs of phonons at critical points in the Brillouin zone are identified, and their stress dependence, especially for the 2TA overtone, is investigated.

I. INTRODUCTION

Recently it was found that incipient ferroelectrics such as $KTaO_3$ and $SrTiO_3$ undergo ferroelectric phase transition under a uniaxial pressure.[1-3] Low-frequency dielectric measurements at liquid-helium temperatures showed that, under the uniaxial pressure, the dielectric constants of these materials become highly anisotropic, and one of these diverges at a critical pressure, where the second-order ferroelectric phase transition takes place. Raman-scattering study of $SrTiO_3$ under the uniaxial pressure revealed various aspects of the soft phonon modes, especially pressure characteristics of the frequencies and the linewidths of the ferroelectric phonons.[3] On the basis of Landau-Devonshire phenomenological theory, this phase transition is well described by the free-energy function including the electrostrictive effect.[1,3] In a lattice-dynamical viewpoint that the anomalously low frequency of the soft phonon originates from the balance between the short- and long-range forces,[4] this induced phase transition may be understood as a result of the reduction of the short-range restoring force between ions owing to the lattice expansion in the plane perpendicular to the stress axis.

In this paper we investigate the uniaxial stress-induced ferroelectricity of $KTaO_3$ by observing phonon behaviors under the stress by means of Raman scattering. For the induced ferroelectric phase transition, we have determined the crystallographic direction and magnitude of the induced spontaneous polarization, and values of nonlinear dielectric coefficients. Although the linewidth of the total symmetric soft mode has been found to anomalously increase near the transition pressure, the line shapes are well described by a simple damped harmonic oscillator with a small damping factor. Thus this phase transition will provide a typical example of the ferroelectric phonon condensation in the perovskite oxides. In addition, we investigate the stress dependence of higher-frequency phonons, involving other zone-center phonons and pairs of phonons at critical points in the Brillouin zone.

II. THEORY

Previously we showed that, under the uniaxial stress along the pseudocubic axis, values of dielectric constant decrease along the stress axis but increase in the plane perpendicular to the stress axis,[1] and thus the crystal symmetry becomes tetragonal D_{4h} from cubic O_h. The pressure coefficient of the inverse dielectric susceptibility gives the electrostrictive coefficient value. Further application of the stress leads to the ferroelectric phase transition which is indicated by the fact that the dielectric constant in the plane perpendicular to the stress axis takes a peak value near the transition pressure $\sigma_c = 5.6$ kbar. The direction of the spontaneous polarization in this phase, however, could not be determined in the previous study of the dielectric measurement.[1] The present Raman-scattering study will show that the polarization develops along the $\langle 100 \rangle$ direction, and symmetry of this ferroelectric phase should be orthorhombic C_{2v}.

A. Symmetry of the phonon

In the cubic O_h phase, there are three F_{1u}- and one F_{2u}-type modes. The F_{1u} modes are infrared active and therefore split into TO and LO modes. Experiments (Sec. III A) will show that only the lowest-frequency TO modes remarkably change their frequencies under the pressure. In Table I are shown symmetry changes of these soft modes

TABLE I. Symmetry of the soft ferroelectric modes under the (010) stress.

O_h	D_{4h} ($\sigma<\sigma_c$)	C_{2v} ($\sigma>\sigma_c$)	Polarizability tensor [a]	
F_{1u}	$A_{2u}(y)$	$B_2(y)$	$\alpha_{yz}\alpha_{zy}$	$\alpha_{XY}\alpha_{YX}\alpha_{YZ}\alpha_{ZY}$
	$E_u(x,z)$	$A_1(z)$	$\alpha_{xx}\alpha_{yy}\alpha_{zz}$	$\alpha_{XX}\alpha_{YY}\alpha_{ZZ}$
		$B_1(x)$	$\alpha_{zx}\alpha_{xz}$	$\alpha_{XX}\alpha_{ZZ}$

[a]Small letter subscripts refer to crystallographic pseodocubic axes, and capital letter subscripts refer to the coordinate axes rotated around the stress Y axis by 45° (see Fig. 1).

under the uniaxial pressure along the pseudocubic y direction. The direction of the polarization of the mode is denoted in parentheses. At the critical pressure σ_c, the frequency of the $E_u(x,z)$ mode will vanish and the spontaneous polarization will develop along the pseudocubic [100] or [001] direction. In the ferroelectric phase, we denote the direction of the spontaneous polarization by z. Then the frequency of the total symmetric $A_1(z)$ mode in the C_{2v} phase will become harder with increase of the pressure. All the modes become Raman active in this C_{2v} phase. In our experiments, directions of the incident laser and scattered light are confined in the xz plane perpendicular to the stress y axis, which allows Raman-scattering observation of the $B_2(y)$ and $A_1(z)$ modes, but not of $B_1(x)$ mode, which could be observable only in the back-scattering geometry of the laser beam along the stress y axis. But by some reasons mentioned in Sec. III A, we were able to observe the $B_1(x)$ mode. It is noted that the "silent" F_{2u} mode in the cubic O_h phase turns to the Raman-active A_1, B_1, and B_2 modes in the C_{2v} phase.

B. Frequency of the soft ferroelectric phonon

The vibrational displacement associated with the lowest-frequency TO phonon was determined by a neutron experiment[5] as a "Slater-type" one, in which the Ta ions move against the oxygen octahedra along a pseudocubic axis. Then, we take the amplitude of the Ta ions as $u_{\mathrm{Ta}} = 3m_0(m_{\mathrm{Ta}}+3m_0)^{-1}w$, and that of the oxygen ions as $u_0 = -m_{\mathrm{Ta}}(m_{\mathrm{Ta}}+3m_0)^{-1}w$, where m_{Ta} and m_0 denote the mass density of the Ta and O ions. The polarization P and the harmonic energy density U associated with this mode can be written as follows:

$$vP = \sum u_i Q_i = e^* W , \tag{1}$$

$$U = \sum m_i \omega^2 u_i^2 = m_p \omega^2 w^2 , \tag{2}$$

where

$$e^* = [\,3m_0 Q_{\mathrm{Ta}} - m_{\mathrm{Ta}}(Q_{0\parallel} + 2Q_{0\perp})]/(m_{\mathrm{Ta}}+3m_0) , \tag{3}$$

$$m_p = 3m_{\mathrm{Ta}}m_0/(m_{\mathrm{Ta}}+3m_0) . \tag{4}$$

Here Q's denote the apparent charges of the ion defined by Cochran[6] and v is the unit-cell volume. Equations (1) and (2) indicate that the ferroelectric mode is regarded as an oscillator with characteristics of the amplitude $(v/e^*)P$, the mass density m_p, and the effective charge e^*. Hence, we can derive the expression of the ferroelectric mode frequency ω_i from Helmholtz's free energy A expressed as a power series[3] of P (the explicit forms of the free-energy functions A and G are written in the Appendix):

$$\omega_i^2 = m_p^{-1}\left(\frac{e^*}{v}\right)^2\left(\frac{\partial^2 A}{\partial P_i^2}\right)\Bigg|_{eq} = Z^2\gamma_i \quad (i=x,y,z) , \tag{5}$$

where $\gamma_i \equiv 4\pi/(\epsilon_i - 1)$ denotes the inverse dielectric susceptibilities in the clamped state and $Z^2 \equiv m_p^{-1}(e^*/v)^2$. This expression (5) is in accordance with the Lyddane-Sachs-Teller (LST) relation. γ_i is given as a function of the uniaxial pressure load σ as follows:

For the paraelectric phase ($\sigma<\sigma_c$),

$$\begin{aligned} &\gamma_{x,z} = \gamma_0 + 2Q_{12}\sigma = 2Q_{12}(\sigma-\sigma_c) \quad (E_u \text{ mode}) , \\ &\gamma_y = \gamma_0 + 2Q_{11}\sigma \quad (A_{2u} \text{ mode}) , \\ &\sigma_c \equiv -\gamma_0/(2Q_{12}); \end{aligned} \tag{6}$$

and for the ferroelectric phase ($\sigma>\sigma_c$),

$$\begin{aligned} &\gamma_z = 8D^X P_s^2 \quad (A_1 \text{ mode}) , \\ &\gamma_x = (2D_n^X + g_{44}^2/c_{44})P_s^2 \quad (B_1 \text{ mode}) , \\ &\gamma_y = \gamma_0 + 2Q_{11}\sigma + (4D^X + 2D_n^X + g_{44}^2/c_{44})P_s^2 \quad (B_2 \text{ mode}) , \end{aligned} \tag{7}$$

where the magnitude of the spontaneous polarization P_s is

$$P_s^2 = (-Q_{12}/2D^X)(\sigma-\sigma_c) , \tag{8}$$

and $Q_{\lambda\mu}$ and $g_{\lambda\mu}$ denote the electrostrictive coefficients in the Gibbs and Helmholtz free-energy functions, respectively. D and D_n, respectively, denote the coefficients of the spherical and anisotropic quartic terms of P in the free energy, and superscripts x and X mean that the coefficients are observed under the "clamped-" and "free-" crystal conditions, respectively. $c_{\lambda\mu}$ denotes the elastic stiffness (see the Appendix).

III. EXPERIMENT

Raman-scattering experiments were done with an Ar^+ laser source (4880 Å), employing the same method as was used for the analogous experiment on $SrTiO_3$, the details of which are described in Ref. 3. The crystal used in the present experiment was grown by the top-seeded solution-growth method. The sample was cut from the same boule as was used for dielectric measurements. Uniaxial stress was applied to the (010) faces. In the right-angle scattering geometry for observing the pure and oblique TO phonons, we cut and optically polished the (101) and ($\bar{1}$01) faces and the (100) and (001) faces, respectively (see Fig. 1). The polished surfaces were prepared by grinding successively with finer grits of alumina followed by finishing with a polishing machine (the AB vibromet polisher, Buehler Ltd.). The size of the sample was ca. $1.5 \times 1.5 \times 7$ mm^3. The sample and the pressing blocks were directly immersed in liquid helium below 2 K for avoiding helium-gas bubbles.

A. Ferroelectric modes

Figure 2 shows low-frequency parts of Raman spectra (0–100 cm^{-1}) as a function of the (010)(Y) pressure load with the incident laser beam directed along [101](X) and scattered light along [10$\bar{1}$](Z). At the stresses larger than σ_c (5.6 kbar from the dielectric measurements[1]), the Raman lines due to soft phonons can be seen. Just above σ_c (6 kbar), this appears as only a shoulder of the exciting laser line. With increasing pressure, this shoulder shifts to higher frequency to grow into an intense Raman line (6.9–7.7 kbar), which decomposes into two lines at higher pressure (8.7 kbar). One can find another stress-sensitive line (60 cm^{-1} at 8.7 kbar) in the ferroelectric phase. We can assign these lines as due to the ferroelectric $B_1(x)$, $A_1(z)$, and $B_2(y)$ modes in order of frequency by using the LST relation and the values of dielectric constants.[1] The scattering geometry $X(YY)Z$, however, allows only observation of $A_1(z)$ mode, as can be seen from Table I. The appearance of the $B_1(x)$ and $B_2(y)$ modes in these spectra might be attributed to the symmetry lowering due to the lattice imperfection or to the small misalignment of the sample. More intense $B_2(y)$ mode scatterings were observed in the $X(ZY)Z$ and $X(YX)Z$ geometry in accordance with the Raman selection rule (Table I). These Raman profiles can be reproduced by a superposition of scatterings of damped harmonic oscillators[3]

$$I_i(\omega) \propto \Gamma_i \omega / [(\omega^2 - \omega_{0i}^2)^2 + \Gamma_i^2 \omega^2] , \tag{9}$$

over the background scattering due to the skirts of the laser and the 2TA peak. Through a course

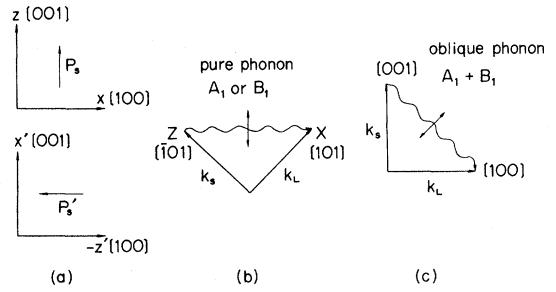

FIG. 1. Right-angle scattering geometries for observing the pure and oblique phonons: (a) two possible directions of the spontaneous polarization; (b) scattering by pure (nonoblique) phonon; (c) scattering by oblique phonon.

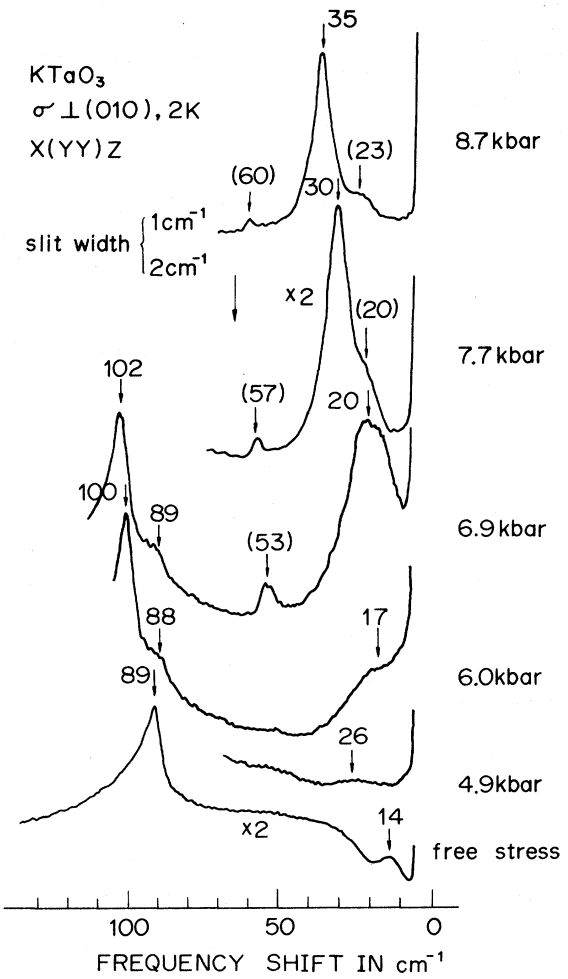

FIG. 2. Variation of the Raman spectra in the low-frequency region as a function of the (010) stress load.

of the least-square-fit method,[7] we could obtain the undamped frequency ω_{0i} and the damping constant Γ_i of the respective modes. Figure 3 shows an example of the Raman spectrum separated into three modes and the background, where the spectrometer slit function is assumed as a triangle one. The obtained values of ω_{0i} are plotted in Fig. 4 as a function of pressure. At the pressure below 7 kbar, it was difficult to separate the lowest peak into the A_1 and B_1 modes, since near σ_c they get closer and linewidths broaden. The solid lines in Fig. 4 represent the best-fit results of Eqs. (5) and (7):

$$\omega[A_1(z)] = (19.0 \pm 0.2)\,(\sigma - \sigma_c)^{1/2}\,,$$
$$\omega[B_1(x)] = (12.5 \pm 0.2)\,(\sigma - \sigma_c)^{1/2}\,, \qquad (10)$$
$$\omega[B_2(y)] = (20.0 \pm 1.1)\,(\sigma + 0.15 \pm 0.86)^{1/2}\,,$$
$$\sigma_c = 5.25 \pm 0.07 \text{ kbar}\,, \qquad (11)$$

where units of σ and ω are in kbar and cm^{-1}, respectively. The value of σ_c coincides with the value of the dielectric measurement (5.6 kbar) within experimental errors. The damping constant of the $A_1(z)$ mode are shown in Fig. 5, where an abrupt increase of Γ near σ_c can be seen. The solid line represents the best fit of Γ to the form $\Gamma = A(\sigma - \sigma_c)^{-n} + B$, where $A = 30$, $B = 6.9$, and $n = 2.7$ (Γ in cm^{-1}, σ in kbar). This divergencelike phenomenon was also found in cases of the stress-induced ferroelectricity in $SrTiO_3$ and many other phase transitions, and the discussion was given in Ref. 3. The Γ values of the B_1 and B_2 Raman lines were found, though the observed results rather scattered, to be essentially constant with the stress

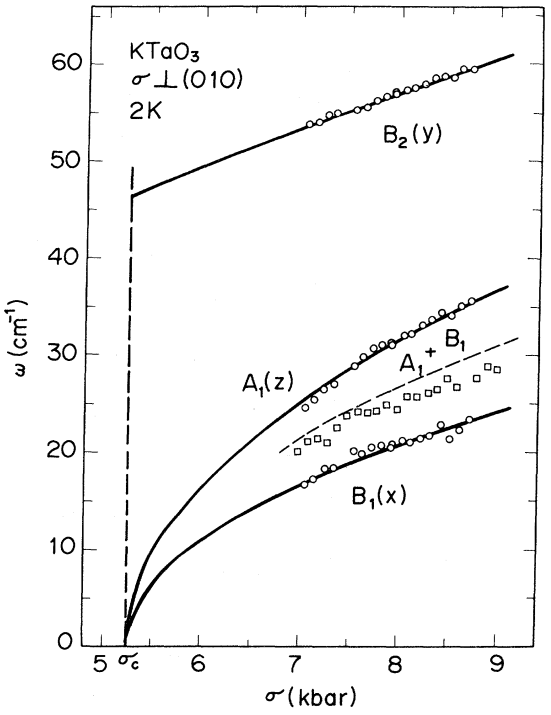

FIG. 4. Frequencies of the soft ferroelectric $A_1(z)$, $B_1(x)$, $B_2(y)$, and oblique A_1+B_1 modes as a function of the (010) stress load. Solid lines are due to the least-square fit for experimental nonoblique phonons (open circles) and a broken line represents theoretical frequencies of the A_1+B_1 mode. Open squares are the observed frequencies of the A_1+B_1 mode.

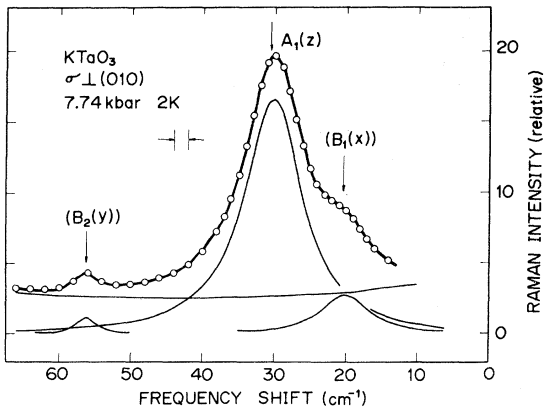

FIG. 3. Decomposition of the low-frequency Raman spectrum into three damped harmonic oscillators and the background. The solid line is the experimental curve and thin lines are the decomposed ones. Open circles represent the sum of the decomposed components.

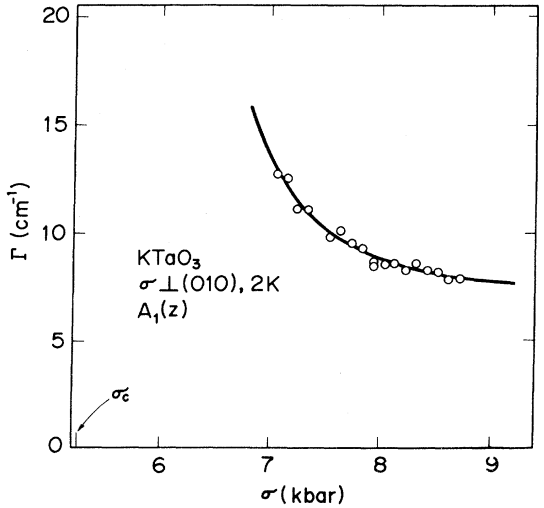

FIG. 5. Stress dependence of the damping constant for the A_1 mode. The solid line represents an empirical formula described in the text.

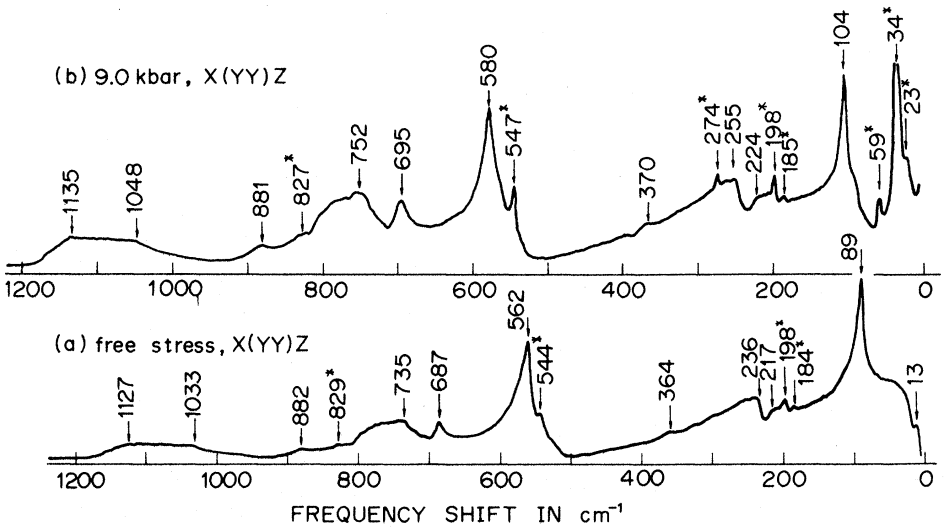

FIG. 6. Raman spectra at 2 K (a) for the free stress and (b) for the stress of 9 kbar. The first-order Raman lines are indicated with an asterisk. The spectra were taken with the slit width of 2 cm^{-1} at 4880 Å.

change.

Foregoing analyses are based on the assumption that the spontaneous polarization develops not along the ⟨101⟩ but along ⟨100⟩ directions in the plane perpendicular to the stress-axis direction. The evidence for this assumption is given by the fact that we have observed two Raman lines of the $A_1(z)$ and $B_1(x)$ types due to phonons directed along ⟨100⟩. Observation of the oblique phonon propagating along the [101] direction [see Fig. 1(c)] will provide a further evidence for the assumption. In this case we have found only one soft Raman line with its frequency[8]

$$\omega_{\mathrm{obl}}^2 = \tfrac{1}{2}(\omega_{A_1}^2 + \omega_{B_1}^2)\,. \tag{12}$$

The obtained frequencies are plotted as a function of pressure in Fig. 4, where a broken line shows the value from Eq. (12) and the experimental frequencies of the $A_1(z)$ and $B_1(x)$ modes. The experimental values of ω_{obl} fall between ω_{A_1} and ω_{B_1}, and near the theoretical estimate. The discrepancy between the experiment and calculation might be ascribed to the misorienting of the sample.

B. Other zone-center modes

Raman spectra up to 1200 cm^{-1} for the paraelectric and stress-induced ferroelectric states are shown in Fig. 6. The spectra include, other than the lines due to the ferroelectric soft modes (cf. Fig. 2), first-order Raman lines due to the zone-center phonons and two-phonons addition band (see Sec. III C). Data of the zone-center-phonon frequency by various experimental methods are shown in Table II. We observed lines at 184,

TABLE II. Frequencies of zone-center phonons in cm^{-1}.

	IR[a] (12 K)	Electric-field-induced Raman[b] (10 K)	Neutron[c] (6 K)	Differential Raman[d] (80 K)	Stressed-induced Raman[e] (2 K)
TO_1	25	18	25		21 ± 3[f]
LO_1	183			188	184
TO_2	196	198		202	198
LO_2/TO_3				282	274
LO_3	421			422	
TO_4	547	556		554	544
LO_4	837			830	829

[a] Reference 10.
[b] Reference 19.
[c] Reference 16.
[d] Reference 9.
[e] Present work.
[f] Value estimated at the free stress by the method described in the text.

TABLE III. Interpretation of the second-order Raman structures for the free or stress-loaded (9 kbar) states in terms of phonons at two critical points. Frequency values for the stressed crystal are written in parentheses. After Yacoby and Linz (Ref. 9), phonon frequencies are separated into two sets (frequency unit in cm^{-1}).

Yacoby and Linz (77 K)	Present work (2 K)	45 (52)	172 (172)	191 (203)	517 (528)
55	45 (52)	89 (104)	217 (224)	236 (255)	562 (528)
173	172 (172)			364 (370)	687 (695)
195	191 (203)				
520	517 (528)				1033 (1048)
		294 (302)	441 (441)		
296	294 (302)		735 (743)		
444	441 (441)		881 (881)		

198, 544, and 829 cm^{-1}, even in the spectrum of the paraelectric state, which might be a result of scattering from regions with local dislocations around impurities.[9] In the stress-induced ferroelectric phase, these lines grow more intense, and one of the lines appreciably changes the frequency (from 544 to 547 cm^{-1} at 9 kbar). The contribution of this frequency change to the dielectric constant in the LST relation is estimated as 1%, so that we can safely ascribe the change of the dielectric constant only to the lowest-frequency TO modes. In addition, we find at 274 cm^{-1} a new line, which did not change the position in the ferroelectric phase. Since the frequency of the line falls between the frequencies of TO_2 and LO_3 phonons, this line can be identified as due to the "silent" F_{2u} mode in the cubic symmetry. The silent mode was found in the mixed-crystal system [255 cm^{-1} in[10] $Na_{0.4}K_{0.6}TaO_3$, 279 cm^{-1} (E) and 275 cm^{-1} (B_1) in[11] $KTa_{0.64}Nb_{0.36}O_3$, and 282 cm^{-1} in[9] $KTa_{0.9}Nb_{0.1}O_3$ and 5-at.%-Li-doped $KTaO_3$]. The present result nearly agrees with the B_1-mode frequency of $KTa_{0.64}Nb_{0.36}O_3$.

C. Second-order spectra

Let us now turn to the second-order spectra in Figs. 2 and 6. In Fig. 6, one can note well-defined Van Hove critical points of the two-phonon energy density of states, though the spectrum in the absence of the stress is found to be essentially the same as the previous result at 8 K.[12] Since the measurements were done at enough low temperatures, the Raman spectra should correspond to only the two-phonon-emission peaks and bands. Yacoby and Linz[9] investigated in detail the critical points of one- and two-phonons density of states by together using differential fluorescence and Raman techniques. We found eight critical points (in their notation $S1, S5, S6, S8, S13, S14, S15$, $S16$) and two more critical points above 1000 cm^{-1}. Frequencies of these critical points can be analyzed in terms of pairs of phonons in the Brillouin zone,[9] as shown in Table III. We find that all the critical-point frequencies become soft with lowering temperature as well as for the case of the zone-center phonons.

Under the uniaxial pressure at 9 kbar, all the critical-point frequencies are found to increase. These values are tabulated in Table III in parentheses. The stress-sensitive change of the critical-point frequencies is in contrast with the slow change of zone-center hard phonons. Yacoby *et al.*[13] reported hydrostatic pressure dependence of these critical-point frequencies at room temperature. It is noted that their pressure coefficients of the frequencies are considerably small by factors of 2–5 in comparison with the present results.

Next, we discuss the stress change of the 2TA overtone, which can be seen in Fig. 2. In the absence of the pressure, the 2TA overtone appears

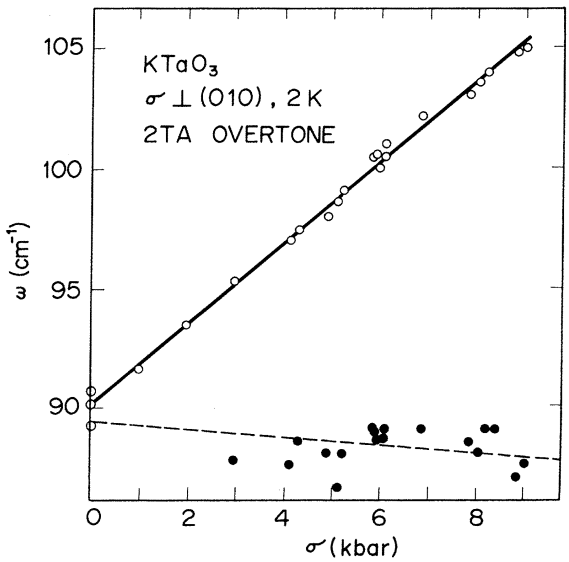

FIG. 7. Stress dependence of the critical-point frequencies corresponding to the 2TA overtone.

at 89 cm^{-1}. A plateau between 20 and 80 cm^{-1} might be due to the TA branch, but the origin of the peak at 14 cm^{-1} is not certain at present.[14] With increasing pressure, the peak of 2TA overtone shifts to higher frequency and a shoulder appears at the lower-frequency side (89 cm^{-1} at 6.9 kbar), which might reflect the change of TA-phonon branches under the uniaxial pressure. The frequencies of the 2TA overtone obtained from the peak and the critical point in the shoulder are plotted as a function of the uniaxial pressure in Fig. 7. The pressure coefficients of the split overtones frequencies exhibit a distinct difference ($d\omega/d\sigma = 1.68 \pm 0.08$ and -0.17 ± 0.12 cm^{-1}/kbar for the upper- and lower-frequencies overtones, respectively). We find no significant change in slope on passing through the phase transition at 5.25 kbar. Neutron scattering experiments for [15-17] $KTaO_3$ and isomorphouse[18] $KNbO_3$ revealed that the phonon energies of the TA branch with the $\langle 100 \rangle$ polarization stay nearly constant in the substantial regions of the Brillouin zone, which gives rise to the intense scattering of the 2TA overtone. Furthermore, for[18] $KNbO_3$ the vibrational displacement was found to consist of essentially the vibration of the B-site atom along the pseudocubic $\langle 100 \rangle$ axis, which might be the case for $KTaO_3$. Therefore, the effect of the uniaxial pressure along the [100] direction should be in two ways: the Ta-ion vibration along the stress axis (case 1) and the Ta-ion vibration perpendicular to the stress axis (case 2). Taking into account of the positive pressure coefficient of the 2TA-overtone frequency in the hydrostatic pressure experiment,[13] the higher-frequency line in Fig. 7 might correspond to the overtone due to the vibration of the case 1, hence the lower-frequency overtone to that of the case 2.

D. Discussion

In this section, we analyze experimental results of the soft ferroelectric phonon on the basis of the phenomenological theory in Sec. II, in order to deduce values of various physical quantities involving the free-stress value of the soft-phonon frequency, the effective charge of the mode, and the nonlinear dielectric coefficient in the free energy.

The free-stress value of the soft-phonon frequency ω_0 can be estimated from the frequency of the $B_2(y)$ mode at σ_c as

$$\omega_0 = \omega_{B_2}(\sigma_c)[-Q_{12}/(Q_{11}-Q_{12})]^{1/2}, \tag{13}$$

which is derived from Eqs. (5) and (6). From the results of Eqs. (10) and (11), $\omega_{B_2}(\sigma_c) = 46.5 \pm 6.6$ cm^{-1}, so that by using values of $Q_{11} = 9.69$ and $Q_{12} = -2.55$ in 10^{-13} cgs,[1] we get $\omega_0 = 21.2 \pm 3.0$ cm^{-1}. This value is in good agreement with the previous data,[10,16,19] as can be seen in Table II.

Next, from Eq. (5), we can evaluate the value of Z^2 [$\equiv m_p^{-1}(e^*/v)^2$] as $(1.63 \pm 0.50) \times 10^5$ $(cm^{-1})^2$, using the above-mentioned ω_0 value and the γ_0 value reported previously as $(2.85 \pm 0.1) \times 10^{-3}$ cgs.[1] Since the quantity Z appears as an effective charge in the expression of the infrared dielectric dispersion function, we can compare our result with infrared experiments,[20,21] which gives $Z = 347$ and 419 cm^{-1} for the "diagonal force" and "diagonal damping" models, respectively. Our result is $Z = 400 \pm 64$ cm^{-1} in agreement with the value due to the diagonal damping model. Furthermore, with the values of $m_p = 0.998$ cgs from Eq. (4), and $v = 6.35 \times 10^{-23}$ cgs, we get $e^* = (4.8 \pm 0.8) \times 10^{-9}$ cgs. On the other hand, the apparent ionic charge Q's can be evaluated by using values of all the infrared-mode charges[22] ($Q_K = 1.2$, $Q_{Ta} = 8.1$, $Q_{O\parallel} = -6.3$, and $Q_{O\perp} = -1.5$ in a.u.). Then, the e^* value is estimated from Eq. (3) as 4.34×10^{-9} cgs, which as a matter of course agrees with the present value.

We then discuss about the pressure dependence of the soft-phonon frequencies. By comparing the experimental results of Eq. (10) with the theoretical equations of (5), (7), and (8), we get the followings in a unit of $(cm^{-1})^2$/kbar:

$$-4Z^2(D^x/D^X)Q_{12} = (19.0 \pm 0.2)^2 \quad (A_1 \text{ mode}), \tag{14}$$

$$-Z^2(2D_n^X + g_{44}^2/c_{44})Q_{12}/(2D^X) = (12.5 \pm 0.2)^2 \quad (B_1 \text{ mode}), \tag{15}$$

$$2Z^2(Q_{11}-Q_{12}) - Z^2(2D_n^X + g_{44}^2/c_{44})Q_{12}/(2D^X) = (20.0 \pm 1.1)^2 \quad (B_2 \text{ mode}). \tag{16}$$

From Eqs. (15) and (16), $Z^2(Q_{11}-Q_{12}) = 122 \pm 24$ $(cm^{-1})^2$/kbar, which is smaller than the value $Z^2(Q_{11}-Q_{12}) = 199 \pm 61$ $(cm^{-1})^2$/$kbar^2$ evaluated using the Z value described above. This discrepancy might indicate the existence of the saturation frequency of the soft mode,[23] since the B_2-mode frequencies are sufficiently high. For the A_1 and B_1 modes, substitution of the Z and Q_{12} values into Eqs. (14) and (15) yields

$$D^x/D^X = 2.4 \pm 0.8, \tag{17}$$

$$(2D_n^X + g_{44}^2/c_{44})/D^X = 8.4 \pm 2.8. \tag{18}$$

Since the following relations hold between D_n^x, D_n^X, D^x, and D^X,[1]

$$D^X = D^x - \tfrac{1}{6}(c_{11}+2c_{12})^{-1}(g_{11}+2g_{12})^2 - \tfrac{1}{3}(c_{11}-c_{12})^{-1}(g_{11}-g_{12})^2, \tag{19}$$

$$D_n^X = D_n^x + (c_{11}-c_{12})^{-1}(g_{11}-g_{12})^2 - (2c_{44})^{-1}g_{44}^2, \tag{20}$$

we can get values of D's and D_n's as

$$D^X = (1.9 \pm 1.0) \times 10^{-12}, \quad D^x = (3.6 \pm 1.1) \times 10^{-12},$$

$$D_n^X = (6.3 \pm 2.3) \times 10^{-12}, \quad D_n^x = (1.8 \pm 2.2) \times 10^{-12},$$

in units of cgs, where we used values of $g_{11} = 3.5$, $g_{12} = -0.2$, $g_{44} = 0.4$ cgs,[1] and $c_{11} = 4.31 \times 10^{12}$, $c_{12} = 1.30 \times 10^{12}$, $c_{44} = 1.09 \times 10^{12}$ cgs.[17] The positive value of D^X indicates that the stress-induced phase transition should be of the second kind. The positive value of D_n^X indicates that the spontaneous polarization should be along the pseudocubic ⟨100⟩ direction in agreement with the statement mentioned in Sec. III A. The D value can also be deduced from the electric field dependences of the soft phonon frequency[19] or the dielectric constant.[24] Recent reports,[25,26] however, describe the formation of the surface layer under the strong electric field. Previous data by these means ($D^X = 3.1 \times 10^{-12}$, $D_n^X = 3.1 \times 10^{-12}$ cgs at 10 K,[19] and $D^X = 2.8 \times 10^{-12}$ cgs at[24] 4.2 K) are in rough agreement with the present data, though the effect of the surface-layer formation was not taken into account.

The value of the spontaneous polarization can be estimated by using the following relation deduced from Eqs. (5) and (7):

$$P_s^2 = \omega_{A_1}^2 / 8 D^x Z^2 .$$

Thus, at the pressure of 8.25 kbar (3 kbar above σ_c), we get $P_s = 5.7 \pm 1.7$ μC/cm^2. This value is about factor 3 larger than the remanent polarization P_r measured previously.[2]

In summary, we have presented the Raman scattering study of the stress-induced ferroelectricity in $KTaO_3$. Although the external parameter which changes the soft-phonon frequency is the stress instead of the temperature, we have found a typical example of the soft-phonon condensation as well as for the case of $SrTiO_3$. A part of the present results has been analyzed in terms of the phenomenological theory, but in future, lattice-dynamical or microscopic studies are expected to be done on the pressure effect to this anharmonic $KTaO_3$ crystal, and on the problem of the increment of the soft-phonon damping constant near the transition point.

ACKNOWLEDGMENTS

The authors wish to thank H. Unoki and Y. Fujii for discussions and K. Oka for his help in growing crystals.

APPENDIX

The Helmholtz's free energy A of the cubic symmetry can be written with the electric polarization P_i ($i = 1, 2, 3$) and the strain x_λ ($\lambda = 1, 2 \ldots, 6$) as follows[1]:

$$A = A_0 + \tfrac{1}{2}\gamma_0 P^2 + D^x P^4 + D^x(P_1^2P_2^2 + P_2^2P_3^2 + P_3^2P_1^2)$$
$$+ \tfrac{1}{2} c_{11}(x_1^2 + x_2^2 + x_3^2) + c_{12}(x_1x_2 + x_2x_3 + x_3x_1) + \tfrac{1}{2} c_{44}(x_4^2 + x_5^2 + x_6^2) - g_{11}(x_1P_1^2 + x_2P_2^2 + x_3P_3^2)$$
$$- g_{12}[x_1(P_2^2 + P_3^2) + x_2(P_3^2 + P_1^2) + x_3(P_1^2 + P_2^2)] - g_{44}(x_4P_2P_3 + x_5P_3P_1 + x_6P_1P_2) .$$

The Gibbs function G under the stress X_λ is

$$G = G_0 + \tfrac{1}{2}\gamma_0 P^2 + D^X P^4 + D_n^X(P_1^2P_2^2 + P_2^2P_3^2 + P_3^2P_1^2) - Q_{11}(X_1P_1^2 + X_2P_2^2 + X_3P_3^2)$$
$$- Q_{12}[X_1(P_2^2 + P_3^2) + X_2(P_3^2 + P_1^2) + X_3(P_1^2 + P_2^2)] - Q_{44}(X_4P_2P_3 + X_5P_3P_1 + X_6P_1P_2) .$$

[1] H. Uwe and T. Sakudo, J. Phys. Soc. Jpn. 38, 183 (1975).
[2] H. Uwe, H. Unoki, Y. Fujii, and T. Sakudo, Solid State Commun. 13, 737 (1973).
[3] H. Uwe and T. Sakudo, Phys. Rev. B 13, 271 (1976).
[4] G. A. Samara and B. Morosin, Phys. Rev. B 8, 1256 (1973).
[5] J. Harada, J. D. Axe, and G. Shirane, Acta Crystallogr. A 26, 608 (1970).
[6] W. Cochran Adv. Phys. 9, 387 (1960).
[7] Y. Nishihara, Bull. Electrotech. Lab. Tokyo 39, 865 (1975).
[8] R. Loudon, Adv. Phys. 13, 423 (1964).
[9] Y. Yacoby and A. Linz, Phys. Rev. B 9, 2723 (1974).
[10] C. H. Perry and N. E. Tornberg, Phys. Rev. 183, 595 (1969).
[11] S. K. Manlief and H. Y. Fan, Phys. Rev. B 5, 4046 (1972).
[12] W. G. Nilsen and J. G. Skinner, J. Chem. Phys. 47, 1413 (1967).
[13] Y. Yacoby, F. Cerdeira, M. Schmidt, and W. B. Holzapfel, Solid State Commun. 14, 1325 (1974).
[14] In the experiments of Nilsen and Skinner (Ref. 12), this was not observed possibly because of the broad slit width (8 cm^{-1}) (whereas in the present report 2 cm^{-1}). With increasing pressure, this peak is found to broaden and become negligibly weak (see Fig. 2, 4.9 kbar), which excludes a possibility of identifying this line as the first-order scattering of the soft TO phonon due to the lattice defect. The depression of the TA brance in the Brillouin zone due to a bilinear coupling between the TA and soft TO branches (Ref. 16) might cause the peak structure of the two-phonon density of states at 14 cm^{-1}.

[15]G. Shirane, R. Nathans, and V. J. Minkiewicz, Phys. Rev. 157, 396 (1967).
[16]J. D. Axe, J. Harada, and G. Shirane, Phys. Rev. B 1, 1227 (1970).
[17]R. Comés and G. Shirane, Phys. Rev. B 5, 1886 (1972).
[18]R. Currat, R. Comés, B. Dorner, and E. Wiesendanger, J. Phys. C 7, 2521 (1974).
[19]P. A. Fleury and J. M. Worlock, Phys. Rev. 174, 613 (1968).
[20]R. C. Miller and W. G. Spitzer, Phys. Rev. 129, 94 (1963).
[21]A. S. Barker, Jr. and J. J. Hopfield, Phys. Rev. 135, A1732 (1964).
[22]J. D. Axe, Phys. Rev. 157, 429 (1967).
[23]G. Shirane and Y. Yamada, Phys. Rev. 177, 858 (1969).
[24]D. Kahng and S. H. Wemple, J. Appl. Phys. 36, 2925 (1965).
[25]U. T. Höchli, Ferroelectrics 7, 237 (1974).
[26]Y. Fujii and T. Sakudo, J. Phys. Soc. Jpn. 41, 888 (1976).